Available online at **www.joac.info**

ISSN: 2278-1862

Journal of Applicable Chemistry

2020, 9 (1): 159-170

(International Peer Reviewed Journal)

A Facile, One-Pot and Eco-Friendly Synthesis of V_2O_5 Nanoparticle for Enhanced Catalytic Reduction of Celestine Blue

C. Sudhakar[1], B. Tamil selvi[2], A. Karthika[2], A. Suganthi[2] and M. Rajarajan[1]*

1. Madurai Kamaraj University, Madurai-625 021, Tamilnadu, **INDIA**
2. PG and Research Department of Chemistry, Thiagarajar College, Madurai-625009, Tamilnadu, **INDIA**

Email: suganthiphd09@gmail.com, rajarajan1962@yahoo.com

Accepted on 20th January, 2019

ABSTRACT

A one-pot synthesis of V_2O_5 nanoparticle using Image result for eucalyptus tree Eucalyptus leaf extracts (G-V_2O_5) as a reducing and stabilizing agent is reported herein. The G- V_2O_5 was synthesized by the co-precipitation method and characterized by X-ray diffraction (XRD), Fourier transform infrared spectroscopy (FT-IR), Field emission scanning electron microscopy (FE-SEM), elemental analysis (EDX) and photocatalytic degradation. The prepared nanoparticles were tetragonal and monoclinic in structure and confirmed by the XRD patterns. The photocatalytic activity of the mixture of 2% G- V_2O_5, 3% G- V_2O_5 and 5% G- V_2O_5 were studied in Celestine Blue degradation reaction. 3% G-V_2O_5 showed the highest photocatalytic activity among the mixtures. The dye Celestine Blue (CB) showed 89 percentage of degradation obtained in180 min with the mixture of G-V_2O_5.

Graphical Abstract

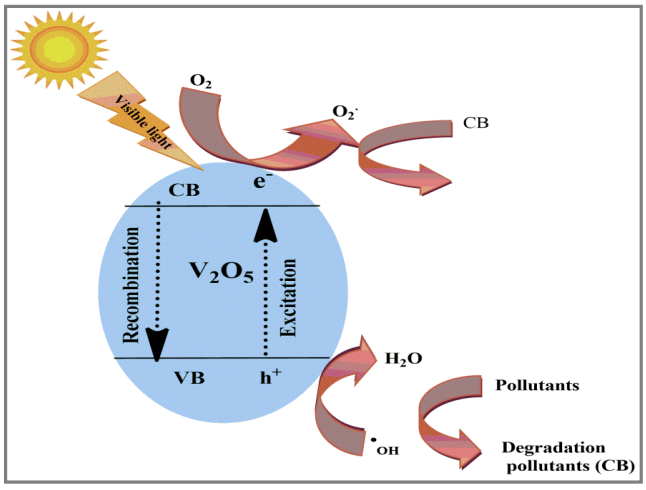

Keywords: Celestine Blue, G-V_2O_5, Photocatalytic activity, Degradation.

INTRODUCTION

In present day, synthetic dyes are considered as a main source for pollution of water including, underlying waters, river water, lake water and drinking waters. Annually large amounts of these dyes dispose from factories into the ambient environment causing pollution of water and soil. The polluting effect of these dyes increase especially when the organic chemical structure of these dyes containing some constituents such as sulfur, nitrates, heavy metals, etc. [**1-3**]. As a result of global warming especially in the industrial states and the shortage of water, the process of treatment of polluted water becomes from essential requirements to reuse this polluted water to be reused for further uses especially for industrial processes. In this context, different methods and techniques can be used for this purpose. These are physical methods, chemical methods and biological methods. In general, most of these methods are not sufficient effective and cost effective [**4**]. Recently, heterogeneous photocatalytic methods were applied as an alternative method that can be used in treatment of polluted waters [**5, 6**].

Many researches had been reported using photocatalysts in heterogeneous photocatalysts systems investigating removal of polluted dyes from industrial waters. Most of these photocatalysts showed higher efficiency in dye removal besides that these photocatalysts can be cyclized to be used more than one time [**7**]. In this context, many types of semiconductors photocatalysts were applied such as TiO2, ZnO, Cu_2O, CdS, ZnS, V_2O_5, HgO etc. in the presence of UV light and solar spectrum with hydrogen peroxide . Also different modified forms of these photocatalyst include doped oxides with metals and non-metals, activated carbons/photocatalysts and coupled oxides [**8-11**]. Vanadium pentoxides (V_2O_5) have newly established considerable attention for a selection of applications due to their unique physicochemical properties [**12**]. They have a variety of hopeful applications including catalysis, photocatalysts, lithium-ion batteries, hydrogen storage material, corrosion prevention, gas sensors, dye-solar cells sensitized, ultraviolet absorbents, conducting electrodes and so forth. Nanomaterials based adsorbents are highly recommended for the removal of dyes. These adsorbents show high surface area and reactive atoms, large and wide dimension pores that can be applied as a new strategy for their efficient application in wastewater treatment [**13**]. V_2O_5 is an important binary semiconductor oxide. Because of its high electron mobility, high electrical conductivity, chemical sensitivity and adequate thermodynamic stability, V_2O_5 finds promising applications in gas sensors, solar cells, anode materials for rechargeable lithium ion batteries and photocatalytic applications [**14-16**]. However, the rapid recombination of photogenerated electron–hole pairs in photocatalytic process diminishes the effective degradation of pollutants. Therefore, many efforts have been explored among the scientific community to overcome this problem [**17**]. One of the important approaches is the coupling of two semiconductors. Using coupled semiconductor photocatalysts enhances the electron–hole separation through the interfacial charge transfer between the semiconductors which substantially improve the photocatalytic activity [**18**].

In this paper, we present a new visible-light driven catalyst G-V_2O_5 were synthesized by a sonochemical method, which shows high photocatalytic activity on photodegradation of organic substrates under visible light irradiation. The structures and the surface morphology were demonstrated by X-ray diffraction (XRD), scanning electron microscopy (SEM), elemental analysis, fourier transform infra red spectroscopy (FT-IR) and energy dispersive x-ray analysis respectively. To evaluate these adsorption behaviors further, solution pH, contact time at different initial concentrations, catalyst dosage and the effects of ultrasound parameters were investigated systematically. The photocatalytic mechanism of G-V_2O_5 nanocomposite under visible light was discussed in detail. However, to the best of our knowledge, until now there is no report on the synthesis of G-V_2O_5 nanocomposites and its exploration for the photocatalytic degradation of CB dye is illustrated in the present investigation.

MATERIALS AND METHODS

Leaf extracts preparation: Fresh and eucalyptus leaves were collected in our college campus and rinsed thoroughly with running tap water followed by distilled water to remove all dust and other contaminated organic contents and cut into little pieces.100 mg of the small pieces of the Eucalyptus leaf leaves were boiled with 100 mL distilled water at 60°C for 30 min and the extract was thrice filtered with No.1 Whatman paper to remove the particulate substance and to obtain a clear solution. The filtrated Eucalyptus leaf was pale green, and it was used as a stabilizing agent as well as reducing for the mixture of the composites. The filtrate solution was stored in the refrigerator at 4°C for further experiment.

Synthesis of G-V_2O_5 nanocomposite: 15 mL of Eucalyptus leaves extract and 3 g of V_2O_5 was dissolved in 50 mL DD water followed by ultrasonication (400W) for 2 h. The obtained solution was stirred with 30 min for magnetic stirrer and the homogenous solution was obtained. The homogenous solution was washed with water, ethanol and dried oven at 80°C for 12 h. Then nanocomposite was calcinated at 200°C for 4 h in air, the G-V_2O_5nanocomposite was obtained.

Photodegradation experiments: Photodegradation experiments were carried out in a cylindrical immersion type photo reactor. The photocatalytic activity was evaluated by monitoring the degradation of dyes under visible light irradiation. 300 mL aqueous solution of dye was taken in a cylindrical glass vessel equipped with a circulating water jacket to cool the lamp and to maintain constant temperature, in which air was bubbling continuously from the bottom of the reactor. Then, pH of the solution was adjusted using 0.1M H_2SO_4 (or) 0.1M NaOH and required amount of photocatalyst was added into the vessel. Before irradiation, the aqueous suspension containing CB photocatalyst was continuously stirred for 30 min in dark to reach an adsorption–desorption equilibrium. After that, the mixture was subjected to visible light irradiation using 150W tungsten lamp. At regular time intervals, 5 mL aliquot of the reaction mixture was collected, centrifuged and filtered through a 0.2 µm to Millipore filter to remove the photocatalyst powder. "C", the absorption of CB photocatalyst solution at irradiation time of 't' min, and "C_0" the initial absorption at t=0 min was calculated.

Instrumentation: Fourier transmission infrared spectroscopy recorded at FT/IR 6600, Jasco spectrometer. Raman spectrometer recorded by using WI-Tech CRM-200. The structure and shape were carried out by FE-SEM Carl Zeiss, Germany (Supra 35-VP) and 15 kV operated. For X-ray diffraction, JEOL JDX with 8030Cu Ka radiation at an operating voltage (40 kV) and a current of 100 mA was used. Photodegradation experiments were performed in a HEBER immersion type photoreactor (HIPR-MP125).

RESULTS AND DISCUSSION

Characterization: Figure 1(a-d) shows the crystallographic nature of the synthesized material was investigated by the X-ray diffraction method. Figure1a shows, the pure V_2O_5 phase (JCPDF 41-1426), corresponds well to the structure of orthorhombic, with lattice parameters such as a=11.516Å, b=3.566Å and c=4.373Å have appeared respectively. Also green supported V_2O_5 nano sheet, while increased with the crystallinity of composite peak was shifted towards 2θ value is higher as illustrated in figure1b-d. Moreover, the diffraction peaks of V_2O_5 and 2% G- V_2O_5, 3% G-V_2O_5 and 5% G-V_2O_5 appear in the curves composites as exposed in figure1, signifying that the three components peaks are successfully hybridized [**19, 20**]. The chemical composition and bond analysis were examined for the as-prepared V_2O_5 and 2% G-V_2O_5,3% G- V_2O_5, 5% G-V_2O_5 nanocomposite was investigated by FT-IR spectrum.

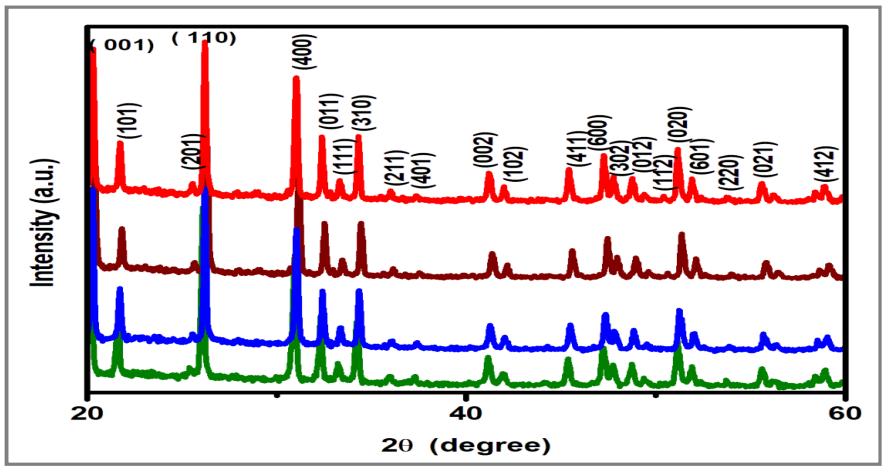

Figure 1. XRD pattern of a) V_2O_5, b) 2% G-V_2O_5, 3% G- V_2O_5, 5% G-V_2O_5 nanocomposite.

The FT-IR spectrum of V_2O_5 (Figure 2a) exhibits indicates the presence of the (V=O) symmetrical peaks appeared at 998 cm^{-1} respectively [21-24]. The peaks at 799 and 533 $cm^{-1}$are assigned to the V-O stretching and V-O-V bending vibration, which may well be ascribed to stretching vibration of the O-H bond of water molecules. As well as another peak at 1600 cm^{-1} assigned to sharp vibration of water molecules. Besides green extract, the broad absorption range at 3,445 cm^{-1} was attributed in the H-O-H band observed in water molecules. The spectrum of green extract describes the peaks at 2,854 cm^{-1} for the incidence of symmetric and asymmetric -CH_2 stretching vibration respectively. Symmetric stretching of carboxylate anion -COO represents an absorption band at 1,641 cm^{-1}. Figure 2 a-d V_2O_5 and G-V_2O_5 (2% G- V_2O_5, 3% G-V_2O_5 and 5% G-V_2O_5), from the peak 3305 to 3000 cm^{-1} is attributed to the stretching vibration modes of N-H bonds resulting from the incomplete condensation of amino groups.

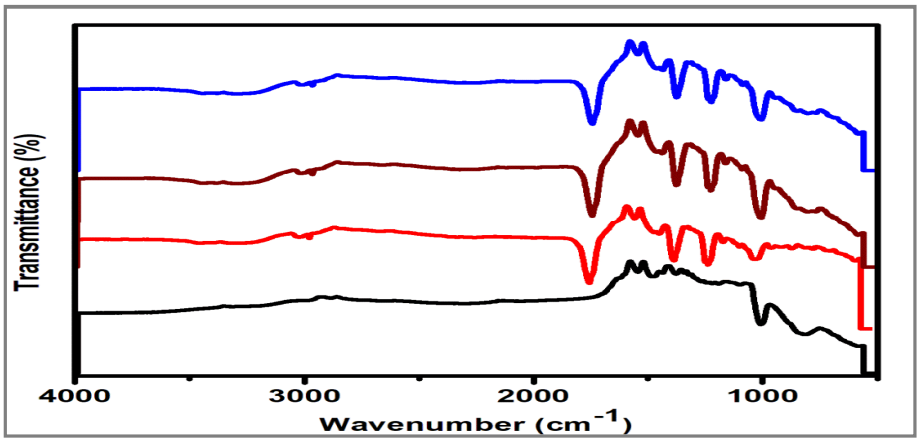

Figure 2. FT-IR spectrum of a) V_2O_5, b) 2% G-V_2O_5, 3% G- V_2O_5, 5% G-V_2O_5 nanocomposite.

Raman spectra of V_2O_5 and 2% G- V_2O_5, 3% G-V_2O_5 and 5% G-V_2O_5 nanocomposites are shown in figure 3. Raman spectrum of the sample was prepared at 500°C, it reveals entire Raman active mode appeared at the seven (993, 692, 527,406, 278, 192, 139 cm^{-1}) frequencies vibration mode shown by figure 3. Figure 3 a-d shows a Raman spectrum of V_2O_5, 2% G- V_2O_5, 3% G-V_2O_5 and 5% G-V_2O_5 which exhibited the strong powerful peak present at 139 cm^{-1} corresponds to the Bg symmetry and the large in vibration frequency at 990 cm^{-1} corresponding to stretching of O-V-O atoms was observed. The bending and stretching vibration mode appeared at 278, 406 and 527 cm^{-1} are consequential beginning the bending mode of V-O band and 692 cm^{-1} stretching mode to correspond to the parallel and perpendicular plane. These defects and disorders were generally fashioned by the

occurrence of heteroatom, which collapses the controlled crystallization of carbon to the lattice structure of hexagonal shape. These disorder and defects was mostly fashioned by the incidence of hetero atoms, which collapses the structured crystallization of carbon to the hexagonal lattice [25].

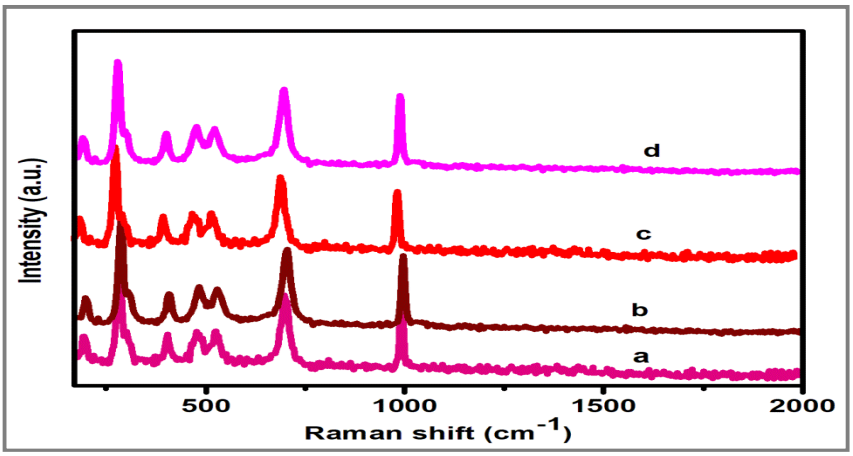

Figure 3. Raman spectra of a)V_2O_5, a) V_2O_5, b) 2% G-V_2O_5, 3% G- V_2O_5, 5% G-V_2O_5 nanocomposite.

The size and morphology of theV_2O_5 and 2% G- V_2O_5, 3% G-V_2O_5 and 5% G-V_2O_5 the nanocomposite are shown in figure 4. FE-SEM image of V_2O_5 (Figure 4a), clearly shows the nanosheet shape. Figure 4b showed the characteristic FE-SEM images of the V_2O_5 agglomerated image for sheet shape and it is randomly distributed. The 3% G-V_2O_5 nanocomposite provides superior exterior area, superior surface motion and well-organized transmission direct for discovery of analytes and helped to achieve the active sites, to improve the sensitivity of the nanocomposite surface modified electrode. Figure 4c is showed corresponding to the EDX spectrum of 3% G-V_2O_5, which confirms the appearance of the following elements such as V, O, C, and N. The EDX spectrum was obtained by a good quality concurrence with the reported nanocomposite investigated by the spectrum of EDX. The elemental coloured mapping images in figure 5(a-d) fairly showed the V (red), O (green), N (yellow) and C (blue) elements in the material without any other significant impurities.

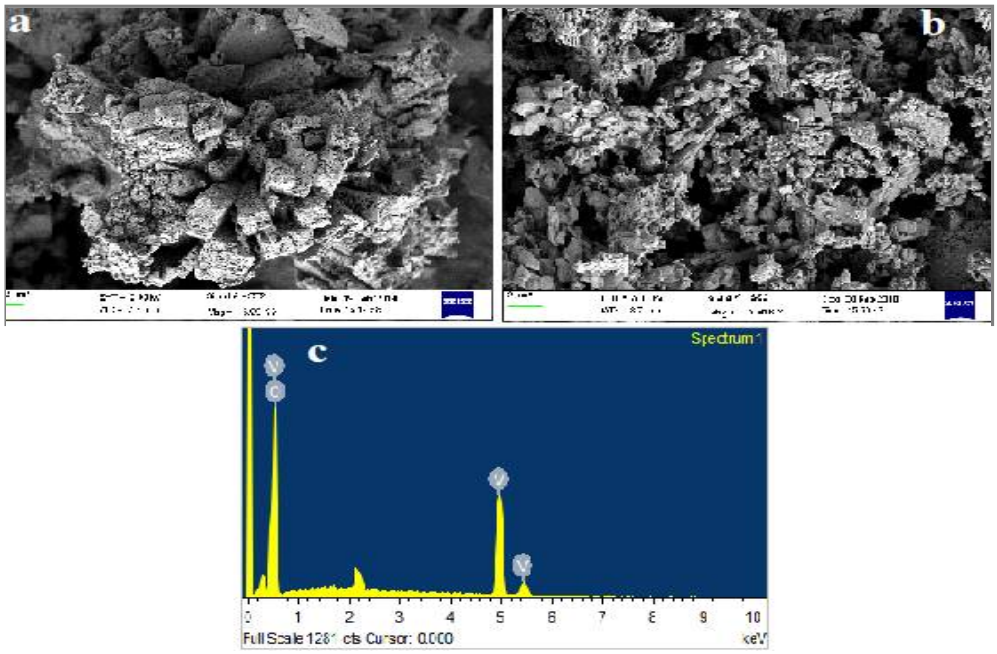

Figure 4. FE-SEM spectrum of a) V_2O_5, b) 3% G- V_2O_5 nanocomposite.

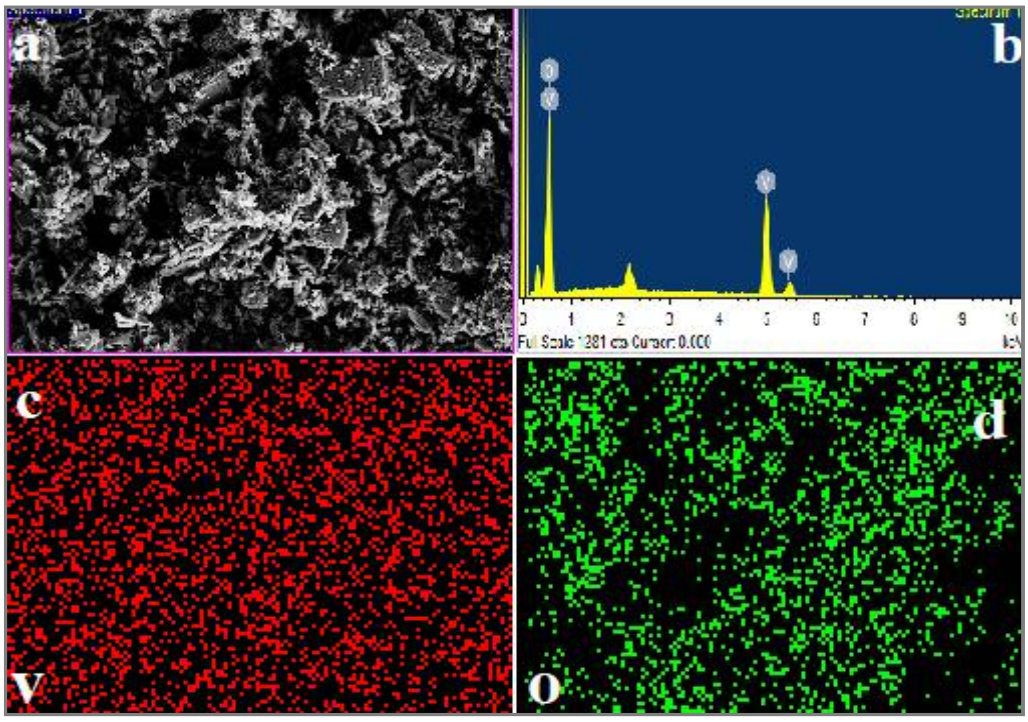

Figure 5. Mapping analysis of 3% G- V_2O_5 nanocomposite.

APPLICATION

Photodegradation studies

Photodegradation of CB: The photodegradation was monitored by examining the variations in maximal absorption with respect to irradiation time in UV-Vis spectra. The photocatalytic activity of 3% G-V_2O_5 semiconductor was investigated by measuring the degradation of CB at pH 6 in the presence of 625 mg L^{-1} catalyst. From these experiments, it was observed that the concentration of CB and the pH play a significant role in photodegradation under visible light irradiation in the presence and even in the absence of the photocatalytic materials [**26**]. The experiment was performed for 30 min under the dark condition in the presence of photocatalytic materials, which indicated the absorption of dye on the active sites of the synthesized photocatalysts with the increase of irradiation time and the absorption peak at λ_{max} 645 nm decreased gradually and after 180 min of irradiation. The photocatalytic degradation of CB in aqueous solution in the presence of 3% G-V_2O_5 resulting in 86% degradation efficiency. No new absorption bands appeared, either in the visible and ultra-violet regions indicating the destruction of the conjugated structure [**27-29**].

According to the previously published literature regarding the photocatalyltic activity of nanocomposites [**19**], we have proposed a mechanism for the enhanced photocatalytic activity of 3% G-V_2O_5. The schematic diagram of electron transfer in 3% G-V_2O_5 visible light irradiation is shown in figure 6. It can be explained as follows: when 3% G-V_2O_5 is irradiated by visible light, V_2O_5 is excited first by photons because of its narrow band gap, which led to the formation of more electrons and holes in its conduction and valance band respectively. The photo generated electrons of V_2O_5 can easily migrate into the conduction band and at the same the holes move in the opposite direction (3% G-V_2O_5) [**30-32**]. Therefore the electron–holes recombination process is highly suppressed and efficient electron-holes separation is achieved on the nanocomposites surface. Simultaneously, the photodegradation of CB is achieved by the capture of conduction band electrons and the holes oxidize H_2O to O_2.

Effect of pH: The effect of pH on the photodegradation of CB was studied in the pH range of 2 to 10 with an initial CB concentration 6 µM, catalyst dosage 625 mg L^{-1}. The results are displayed in figure 7. The Photodegradation of CB increases from pH 2-6 and it decreases as the pH increases to 8. It was adjusted to alkaline or acidic conditions by adding the appropriate amount of NaOH or H_2SO_4 [**33, 34**]. This is due to the change in electrostatic attraction or repulsion between pollutant molecules and catalyst. CB is a cationic dye and therefore the electrostatic attraction between the dye molecules and catalyst is greatly improved at pH 8 [**35**].

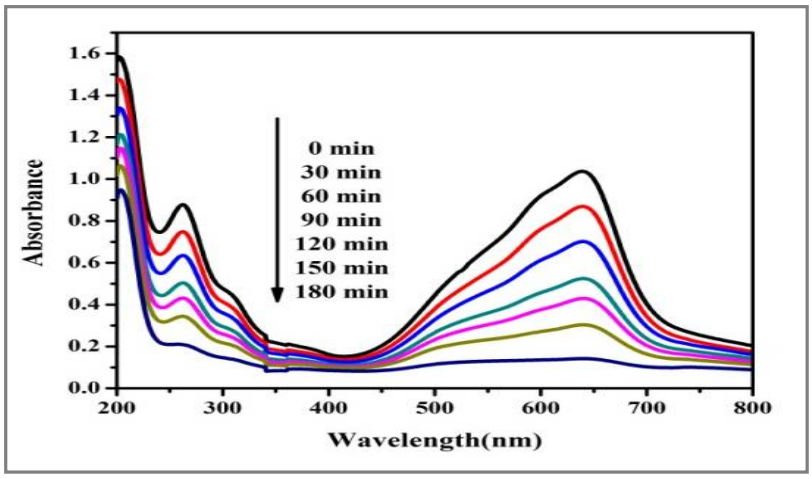

Figure 6. Time Dependent UV-Vis Spectral Changes of CB (6 µM) in Presence of (3% G-V_2O_5) (625 mg L^{-1}).

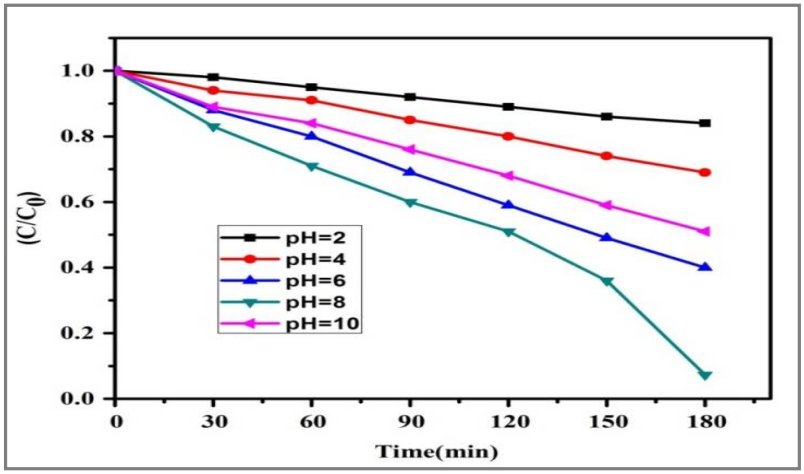

Figure 7. Effect of pH on the photodegradation of CB.

Effect of Catalyst Dosage: In order to optimize the photocatalyst dosage on the degradation of CB, experiments were carried out with varying 3% G-V_2O_5 dosage from 375 mg L^{-1} to 875 mg L^{-1}, at constant CB concentration of 6 µM and pH 8 and the results are shown in figure 8. The photo degradation of CB is negligible in the absence of catalyst. The degradation of CB increased with increase in photocatalyst concentration from 375mg L^{-1} to 500 mg L^{-1} and a further increase in catalyst concentration leads to decrease in photodegradation. This is due to the increase of total active surface area and the availability of more active sites on the catalyst surface for photoreaction [**36-38**].

Effect of Concentration: The effect of initial dye concentration on its photodegradation was investigated from 2 µM to 8 µM, at pH 6 and 3% G-V_2O_5 dosage of 625 mg L^{-1} and the results are shown in figure 9. It is found that the photodegradation decreases with increase of initial CB concentration. At high dye concentrations, the formation of reactive oxygen species on the

photocatalyst surface is reduced because the photons are interrupted by the dye molecules before they can reach the catalyst surface. 3% G-V_2O_5 dosage is also same for all initial CB concentration and thus the formation of •OH remains constant [**39**].

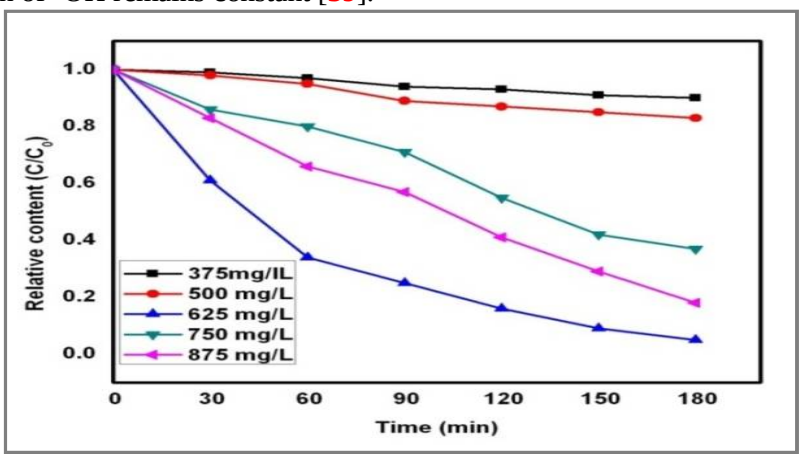

Figure 8. Effect of catalyst dosage on the photodegradation of CB.

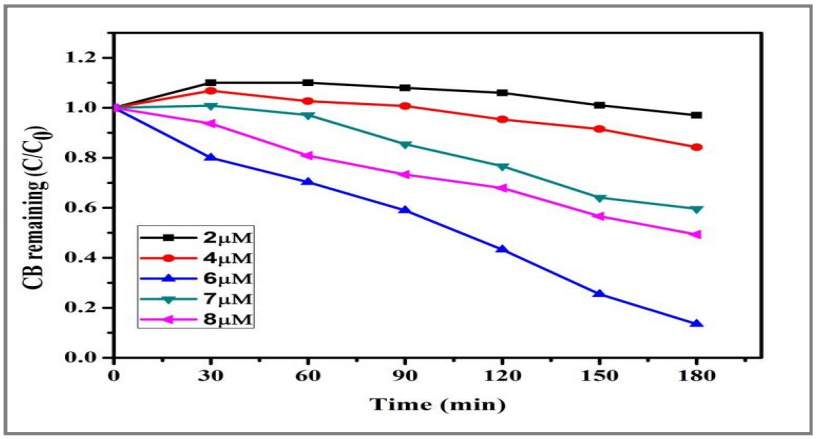

Figure 9. Effect of concentration on the photodegradation of CB.

Kinetics of CB Photodegradation: The kinetics of CB under visible light, over all the photocatalyst was investigated by applying the pseudo-first order equation.

$$-\ln (C_0/C) = kt \qquad ..(5)$$

Here, k is the pseudo-first order rate constant. The plot of $-\ln (C_0/C)$ versus irradiation time (where C_0 is the initial concentration of the dye and C is the concentration of the dye in the reaction time) was found to be linear as shown in figure 10, and this suggests that photodegradation reactions follow pseudo-first order kinetics. The apparent reaction rate constant (k) for the photocatalyltic degradation of CB was evaluated from experimental data using a linear regression, which confirmed the proposed rate law for CB degradation. The apparent rate constants for V_2O_5, 2% G-V_2O_5, 3% G- G-V_2O_5 and 5% G- G-V_2O_5 were determined as $0.0135\times10^{-2}S^{-1}$, $0.225\times10^{-1}S^{-1}$, $0.300\times10^{-1}S^{-1}$and $0.265\times10^{-1}S^{-1}$. The observed results show that 3% G- G-V_2O_5 nanocomposite has higher rate constant than that of other modified and their bare catalysts [**40-42**].

COD: The COD was used as a measure of the oxygen equivalent of the organic content in a sample that was susceptible to oxidation to carbon-dioxide and water by a strong oxidant. The photocatalytic experiments were performed under ideal conditions. Test samples were collected at every 30 min time interval during the process. The COD of the CB before and after the irradiation of visible light was

estimated and shown in table 1. It was observed that the solutions obtained after photodegradation show a significant decrease in COD to 86% after 180 min under the optimum conditions. The results revealed that most of organic matter in CB degrades to smaller species (especially inorganic compounds) and hence the required chemically oxygen demand decreases [**43-45**].

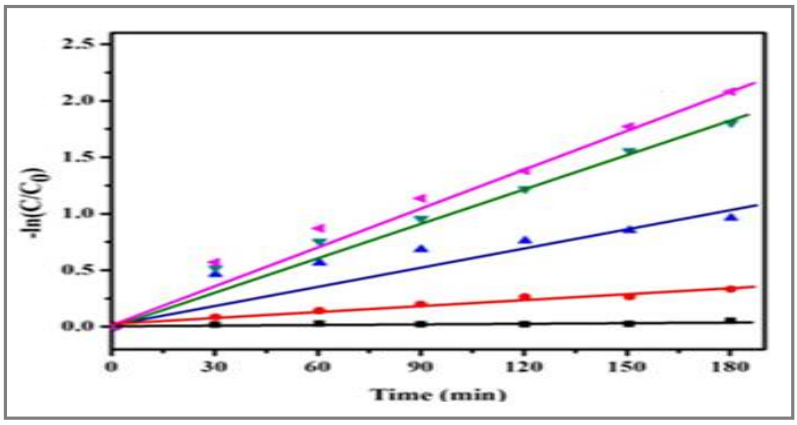

Figure 10. Kinetic regime on the photocatalytic degradation of CB.

Table 1. COD removal (mg L^{-1}) of CB during photodegradation using 3% ZrO_2 –CeO_2 under visible light irradiation

Time (Min)	COD removal Efficiency (%) CB
0	0
30	16.53
60	25.32
90	45.82
120	56.26
150	72.54
180	89.00

Stability and reusability: The reusability of mixture of 3% G-V_2O_5 in photocatalytic activity examined in five-cycles. In the end of each cycle, the catalyst removed, the photocatalyst obtained from the first run was filtered, washed several times with water and dried at 80°C at time of 2 h and reused in following cycle. The degradation of 50% in fifteen-cycle indicates the performance of mixture of 3% G-V_2O_5 as photocatalyst. The same photocatalyst was recycled for four times for the degradation Celestine blue pollutants and the results. The photocatalytic activity of 3% G-V_2O_5 is not diminished even after the fourth cycle. However, there is a small drop in photocatalytic activity at the third and fourth cycles and this may be due to the loss of photocatalyst during washing. The important crystallite phases are almost unchanged. Thus, the photocatalyst is stable and effective for the degradation of organic pollutants in water.

CONCLUSION

In the present study 3% G-V_2O_5nanocomposite were successfully synthesized by precipitation-deposition method. The prepared photocatalyst was characterized by UV-DRS, XRD, SEM, EDAX and IR spectra. 3% G-V_2O_5 was efficiently catalyzed the photodegradation of CB under visible light irradiation. Evaluation and optimization of the effect of pH, catalyst dosage and concentration throughout the COD experiment indicated under the studied conditions pH 6, 625 mg L^{-1}, 3% G-V_2O_5 and 180 min irradiation time favour the COD efficiency. Under the above condition approximately 89% of degradation is achieved within 180 mins of irradiation. This study also showed

the chemical stability and good separability of the prepared composites. The kinetics of photodegradation reactions was correlated with the pseudo-first-order model.

REFERENCES

[1]. X. Liu, W. Li, N. Chen, X. Xing, C. Dong, Y. Wang, Ag-ZnO Heterostructure Nanoparticles with Plasmon-Enhanced Catalytic Degradation for Congo Red under Visible Light, *RSC Advances*, **2015**, 5, 34456-34465.

[2]. S. K. Dutta, S. K. Mehetor, N. Pradhan, Metal semiconductor heterostructures for photocatalytic conversion of light energy, *Journal of Physical Chemical Letters*, **2015**, 6, 936-944.

[3]. M. Xie, L. Jing, J. Zhou, J. Lin, H. Fu, Synthesis of nanocrystalline anatase TiO_2 by onepot two-phase separated hydrolysis-solvothermal processes and its high activity for photocatalytic degradation of rhodamine B, *Journal of Hazardous Materials*, **2010**, 176 (1-3), 139-145.

[4]. Y. Liu, F. Xin, F. Wang, S. Luo, X. Yin, Synthesis, characterization, and activities of visible light-driven Bi_2O_3-TiO_2 composite photocatalysts, *Journal of Alloys and Compounds*, **2010**, 498 (2), 179-184.

[5]. E. AlipanahpourDil, M. Ghaedi, A. M. Ghaedi, A. Asfaram , A. Goudarzi,S. Hajati , M. Soylak, Shilpi Agarwal, Vinod Kumar Gupta, Modeling of quaternary dyes adsorption onto ZnO–NR–AC artificial neural network: Analysis by derivative spectrophotometry, Journal *of Industrial and Engineering Chemistry*, **2016**, 34, 186-197.

[6]. E. AlipanahpourDil, M. Ghaedi, A. Asfarama, S. Hajati, F. Mehrabi, A. Goudarzi, Preparation of nanomaterials for the ultrasound-enhanced removal of Pb^{2+} ions and malachite green dye: Chemometric optimization and modeling, *Ultrasonics Sonochemistry*, **2017**, 34, 677-691.

[7]. E. AlipanahpourDil, M. Ghaedi, A. Asfaram, F. Mehrabi, Application of modificated magnetic nanomaterial for optimization of ultrasound-enhanced removal of Pb^{2+} ions from aqueous solution under experimental design: investigation of kinetic and isotherm, *Ultrasonics Sonochemistry*, **2017**, 36, 409-419.

[8]. A. Asfaram, M. Ghaedi, S. Hajati, A. Goudarzi, E. Alipanahpour Dil, Screening and optimization of highly effective ultrasound-assisted simultaneous adsorption of cationic dyes onto Mn-doped Fe_3O_4-nanoparticle-loaded activated carbon, *Ultrasonics Sonochemistry*, **2017**, 34, 1-12.

[9]. E. AlipanahpourDil, M. Ghaedi, A. M. Ghaedi, A. Asfaram, M. Jamshidi, M. K. Purkait, Application of artificial neural network and response surface methodology for the removal of crystal violet by zinc oxide nanorods loaded on activate carbon: kinetics and equilibrium study, *Journal of the Taiwan Institute of Chemical Engineers*, **2016**, 59, 210- 220.

[10]. M. A. Alpuche-Aviles, Y. Wu, Photoelectrochemical study of the band structure of Zn_2SnO_4 prepared by the hydrothermal method, Journal of American Chemical Society, 2009, 131(9), 3216-3224.

[11]. A. Annamalai, D. Carvalho, K. C. Wilson, M.-J. Lee, Properties of hydrothermally synthesized Zn_2SnO_4 nanoparticles using Na_2CO_3 as a novel mineralizer, *Materials Characterization*, **2010**, 61(9), 873–881.

[12]. J. Zhu, L. Cao, Y. Wu, Y. Gong, Z. Liu, H. E. Hoster, Y. Zhang, S. Zhang, S. Yang, Q. Yan, P. M. Ajayan, R. Vajtai, Building 3D Structures of Vanadium Pentoxide Nanosheets and Application as Electrodes in Supercapacitors, *Nano Lett*, **2013**, 13, 5408−5413.

[13]. M. Xu, X. Zhang, S. Gao, X. Cheng, Z. Rong, Y. Xu, H. Zhao, L. Huo, Construction of mono dispersive vanadium pentoxide hollow spheres via a facile route and triethylamine sensing property, *CrystEng Comm*, **2013**,15 () 10123–10131.

[14]. H. Li, J. Wang, X. Liu, Q. Sun, A.B. Djurisic, M. Xie, Y. Mie, C.Y. Tang, K. Shih, Template-free synthesis of hierarchical hollow V_2O_5 microspheres with highly stable lithium storage capacity, *RSC Adv*, **2017**, 7, 2480-2485.

[15]. J. Liu, F. Li, W. Liu, Xin Li, Effect of calcination temperature on the microstructure of vanadium nitride/nitrogen-doped graphene nanocomposites as anode materials in electrochemical capacitors, *Inorg. Chem. Front*, **2019**, 6, 164-171.
[16]. X. Liu, J.Zeng, H. Yang, K. Zhou, D. Pan, V_2O_5-Based nanomaterials: synthesis and their applications, *RSC Adv*., **2018**, 8, 4014-4031.
[17]. D. Majumdar, M. Mandal, S. K. Bhattacharya, V_2O_5 and its Carbon-Based Nanocomposites for Super capacitor Applications, *Chemelectrochem*, **2019**, 6, 1623-1648.
[18]. M. Sathiya, A. S. Prakash, K. Ramesha, J.M. Tarascon, A. K. Shukla, V_2O_5-Anchored Carbon Nanotubes for Enhanced Electrochemical Energy Storage, *J. Am. Chem. Soc*, 2011,13340, 16291-16299.
[19]. B. Long, M.S. Balogun, L. Luo, Y. Luo, W. Qiu, S. Song, L. Zhang, Y. Tong, Encapsulated Vanadium-Based Hybrids in Amorphous N-Doped Carbon Matrix as Anode Materials for Lithium-Ion Batteries, *Small*, **2017**,13, 1702081.
[20]. N. Shash, Effect of vanadium pentoxide on the electrical, dielectric, and optical properties of poly(vinyl alcohol)/vanadium pentoxide nanocomposites, *Ionics*, **2013**, 19, 1825-1834.
[21]. J. Zhu, L. Cao, Y. Wu, Y. Gong, Z. Liu, H. E. Hoster, Y. Zhang, S. Zhang, S. Yang, Q. Yan, P. M. Ajayan, and R. Vajtai, Building 3D Structures of Vanadium Pentoxide Nanosheets and Application as Electrodes in Supercapacitors, *Nano Lett*, **2013**, 13, 5408−5413.
[22]. Y. Hong, J. Yang, H. Fan, Controllable synthesis of various V_2O_5 micro-/nanostructures as high performance cathodes for lithium ion batteries, *Cryst.Eng Comm*., **2017**, 19, 716-721.
[23]. R. Berenguer, M. O. Guerrero-Pérez, I. Guzmán, J. R. Mirasol, T. Cordero, Synthesis of Vanadium Oxide Nanofibers with Variable Crystallinity and V^{5+}/V^{4+} Ratios, *ACS Omega*, **2017**, 2, 7739-7745.
[24]. K. Tadyszak, Ł. Majchrzycki, Ł. Szyller, B. Scheibe, Preparation and characterization of partially reduced graphene oxide aerogels doped with transition metal ions, *J Mater Sci*, **2018**, 53, 16086–16098.
[25]. K. Takahashi, S. J. Limmer, Y. Wang, G. Cao, Synthesis and Electrochemical Properties of Single-Crystal V_2O_5 Nanorod Arrays by Template-Based Electrodeposition, *J. Phys. Chem. B* **2004**, 108, 9795-9800.
[26]. N. Wetchakun, S. Chaiwichain, B. Inceesungvorn, K. Pingmuang, S. Phanichphant, A.I. Minett, J. Chen, $BiVO_4/CeO_2$ nanocomposites with high visible-light-induced photocatalytic activity, *ACS Appl. Mater. Interfaces*, **2012**, 4, 3718–3723.
[27]. H. P. Li, J. G. Liu, W. G. Hou, N. Du, R. Zhang, X. T. Tao, Synthesis and characterization of g-C_3N_4/Bi_2MoO_6 heterojunctions with enhanced visible light photocatalytic activity, *Appl. Catal., B* **2014**, 160–161, 89–97.
[28]. T. Wang, C. J. Li, J. Y. Ji, Y. J. Wei, P. Zhang, S. P. Wang, X. B. Fan, J. Gong, Reduced graphene oxide (rGO)/$BiVO_4$ composites with maximized interfacial coupling for visible light photocatalysis, *ACS Sustain. Chem. Eng.*, **2014**, 2, 2253–2258.
[29]. K. P. Mishra, P. R. Gogate, Intensification of sonophotocatalytic degradation of p-nitrophenol at pilot scale capacity, *Ultrason. Sonochem*., **2011**, 18, 739–744.
[30]. S.-Z. Wu, C.-H. Chen, W.-D. Zhang, Etching graphitic carbon nitride by acid for enhanced photocatalytic activity toward degradation of 4-nitrophenol, *Chin. Chem. Lett*., **2014**, 25, 1247–1251.
[31]. F. M. D. Chequer, V. de P. Venâncio, M. de L.P. Bianchi, L.M.G. Antunes, Genotoxic and mutagenic effects of erythrosine B, a xanthene food dye, on HepG2 cells, *Food Chem. Toxicol.*, **2012**, 50, 3447–3451.
[32]. P. Mpountoukas, A. Pantazaki, E. Kostareli, P. Christodoulou, D. Kareli, S. Poliliou, S. Mourelatos, V. Lambropoulou, T. Lialiaris, Cytogenetic evaluation and DNA interaction studies of the food colorants amaranth, erythrosine and tartrazine, *Food Chem. Toxicol*., **2010**, 48, 2934–2944.
[33]. E. E. Ritchie, J. I. Princz, P. Y. Robidoux, R. P. Scroggins, Ecotoxicity of xanthene dyes and a non-chlorinated bisphenol in soil, *Chemosphere* **2013**, 90, 2129–2135.

[34]. D. P. Das, R. K. Barik, J. Das, P. Mohapatra, K. M. Parida, Visible light induced photo hydroxylation of phenol to catechol over RGO–Ag_3VO_4 nanocomposites without the use of H_2O_2, *RSC Adv*., **2012**, 2, 7377–7379.
[35]. S. Sharma, M. K. Sharma, N.Chaturvedi, Use of ammonium phosphomolybdate as photocatalyst for degradation of celestine blue b, J. Ind. Pollut. Control, **2011**, 2, 0976-5689.
[36]. M. A. Rauf, S. S. Ashraf, Survey of recent trends in biochemically assisted degradation of dyes, *Chemical Engineering Journal*, **2012**, 209, 520-530.
[37]. M. Roushani, M. Mavaei, A. Daneshfar, H. R. Rajabi, Application of graphene quantum dots as green homogenous nanophotocatalyst in the visible-light-driven photolytic process, Journal ofMaterials Science, *Materials in Electronics*, **2017**, 28, 5135–5143.
[38]. P. Kumawat, M. Joshi, R. Ameta, C. Ameta, Photocatalytic degradation of basic Fuchsin over quaternary oxide iron zinc cuprate ($FeZn_2cu_3O_6$), *Advances in Applied Science Research*, **2015**, 6, 209-215.
[39]. K. Ikarashi, J. Sato, H. Kobayashi, N. Saito, H. Nishiyama, Y. Inoue, Photocatalysis for Water Decomposition by RuO_2-Dispersed $ZnGa_2O_4$ with d^{10} Configuration, *The Journal of Physical Chemistry B*, **2002**, 106, 9048-9053.
[40]. L. Balasubramaniam , M. D. H. Wirzal , Z. A. Putra, N. A. H. M. Hadi, M. R. Bilad, Kinetic Study on Celestine blue dye removal using electrocoagulation method, *International Journal for technological research in engineering*, **2018**, 2347 – 4718.
[41]. S. H. Kadhm, T. H. Mgheer, H. I. Ismael, K. J. Kadem, A. S. Abbas, A. J. Atiyah, I. J. Mohamad, Synthesis, Characterization and Catalytic Activity of NiO-CoO-MgO Nano-Composite Catalyst, *Indonesian Journal of Chemistry*, 2019, 19, 2460-1578.
[42]. Selvaraj, Devi, Vairaperumal, Tharmaraj, Quatum dots in photocatalytic application for degradation of Environment pollutants and hydrogen Evaluation, *Green Photocatalytic for energy and environment Process*, **2019**, 1, 87-108.
[43]. E. A. Di, M.Ghaedi, A.Asfaram, Optimization of dispersive liquid–liquid microextraction by microvolume spectrophotometry method to determination of Celestine blue in water sample: response surface methodology, *Frontiers in chemical research*, **2019**, 1, 25-30.
[44]. J. C. R. Angeles, Z. Matamoros-Veloz, J. López-Cuevas, R. Perez-Garibay, J. Diaz-Algarad, K. Yanagisawae, Rotary-hydrothermal method assisting the conversion of celestine into scheelite $SrWO_4$ in alkaline solutions, *International Journal of Mineral Processing*, **2016**, 148, 105-115.
[45]. L. Balasubramaniam, M. D. H. Wirzal , Z. A. Putra , N. A. H. M. Hadi, M. R. Bilad, Kinetic study on celestine blue dye removal usingelectrocoagulation method, *International Journal for Technological Research In Engineering*, **2018**, 2347 – 4718.